Spectral Mixture Analysis of the Urban Landscape in Indianapolis with Landsat ETM+ Imagery

Dengsheng Lu and Qihao Weng

Abstract

This paper examines characteristics of urban land-use and land-cover (LULC) classes using spectral mixture analysis (SMA), and develops a conceptual model for characterizing urban LULC patterns. A Landsat Enhanced Thematic Mapper Plus (ETM+) image of Indianapolis City was used in this research and a minimum noise fraction (MNF) transform was employed to convert the ETM+ image into principal components. Five image endmembers (shade, green vegetation, impervious surface, dry soil, and dark soil) were selected, and an unconstrained least-squares solution was used to un-mix the MNF components into fraction images. Different combinations of three or four endmembers were evaluated. The best fraction images were chosen to classify LULC classes based on a hybrid procedure that combined maximum-likelihood and decision-tree algorithms. The results indicate that the SMA-based approach significantly improved classification accuracy as compared to the maximum-likelihood classifier. The fraction images were found to be effective for characterizing the urban landscape patterns.

Introduction

Urban landscapes are typically composed of features that are smaller than the spatial resolution of the sensors, a complex combination of buildings, roads, grass, trees, soil, water, and so on. Strahler, *et al.* (1986) described H- and L-resolution scene models based on the relationships between the size of the scene elements and the resolution cell of the sensor. The scene elements in the H-resolution model are larger than the resolution cell and can, therefore, be directly detected. In contrast, the elements in the L-resolution model are smaller than the resolution cells, and are not detectable. When the objects in the scene become increasingly smaller relative to the resolution cell size, they may be no longer regarded as objects individually. Hence, the reflectance measured by the sensor can be treated as a sum of interactions among various classes of scene elements as weighted by their relative proportions (Strahler, *et al.*, 1986). Landsat Thematic Mapper (TM) or Enhanced Thematic Mapper Plus (ETM+) images with a nominal 30 meter spatial resolution are attributed to L-resolution model. These data are often considered too coarse for mapping the components of urban environments. As the spatial resolution interacts with the fabric of urban landscapes, a special problem of mixed pixels is created, where several land-use and land-cover (LULC) types are contained in one pixel. Such a mixture becomes especially prevalent in residential areas where buildings, trees, lawns, concrete, and asphalt can all occur within a pixel. Mixed pixels have been recognized as a problem affecting the effective use of remotely sensed data in LULC classification and change detection (Fisher, 1997; Cracknell, 1998). Fisher (1997) summarized four causes of the mixed pixel problem, i.e., (1) boundaries between two or more mapping units, (2) the intergrade between central concepts of mappable phenomena, (3) linear sub-pixel objects, and (4) small sub-pixel objects. When mixed pixels occur, pure spectral responses of specific features are confused with the pure responses of other features, leading to the problem of composite signatures (Campbell, 2002).

The low accuracy of LULC classification in urban areas is largely attributed to the mixed pixel problem. For example, the traditional per-pixel classifiers, such as maximum-likelihood classifier (MLC), cannot effectively handle complex urban landscapes and the mixed pixel problem. When unsupervised classification is applied to densely populated suburban metropolitan areas, the mixed pixel problem becomes exaggerated. Trees on lawns are confused with forest classes. Lawns are similar to pasture and recreation, and pavement is common in high-density residential and commercial/industrial areas (Epstein, *et al.*, 2002). In practice, accurate classification results are a prerequisite for many environmental and socioeconomic applications, such as urban change detection (Chen, *et al.*, 2000; Ward, *et al.*, 2000), urban heat islands (Lo, *et al.*, 1997; Quattrochi, *et al.*, 2000; Weng, 2001), and estimation of biophysical, demographic, and socioeconomic variables (Lo, 1995; Thomson and Hardin, 2000). Improving LULC classification accuracy has been an important theme in remote sensing literature.

Different approaches have been used to improve urban LULC classification or change detection accuracies. These approaches include incorporation of geographic data (Harris and Ventura, 1995), census data (Mesev, 1998), texture features (Myint, 2001; Shaban and Dikshit, 2001), and structure or contextual information (Gong and Howarth, 1990; Stuckens, *et al.*, 2000) into remote sensing spectral data, use of expert systems (Stefanov, *et al.*, 2001; Hung and Ridd, 2002) and fuzzy classification (Zhang and Foody, 2001), use of multi-sensor data such as merged radar and TM data (Haack, *et al.*, 2002), merged SPOT and TM data (Gluch, 2002), and merged

Dengsheng Lu is with the Center for the Study of Institutions, Population, and Environmental Change, Indiana University, Bloomington, IN 47408 (dlu@indiana.edu).

Qihao Weng is with the Department of Geography, Geology, and Anthropology, Indiana State University, Terre Haute, IN 47809 (geweng@isugw.indstate.edu).

Photogrammetric Engineering & Remote Sensing
Vol. 70, No. 9, September 2004, pp. 1053–1062.

0099-1112/04/7009–1053/$3.00/0

TABLE 1. A SUMMARY OF PREVIOUS METHODS USED FOR IMPROVING URBAN LULC CLASSIFICATION ACCURACY

No.	Category	Datasets Used	Study Area	References
1	Use of advanced classifiers	(1) TM (fuzzy) (2) TM (ECHO) (3) ASTER (support vector machine-based algorithm)	(1) Edinburgh (2) Minneapolis, St. Paul, Minnesota (3) Beer Sheva, Israel	(1) Zhang and Foody, 2001 (2) Stuckens *et al.*, 2000 (3) Zhu and Blumberg, 2002
2	Use of sub-pixel information	(1) TM and aerial photographs (2) IRS-1C multispectral and panchromatic image	(1) Southeast Queensland, Australia (2) Metropolitan area of Cairo, Egypt	(1) Phinn *et al.*, 2002 (2) Rashed *et al.*, 2001
3	Incorporation of spectral and spatial information	(1) SPOT (2) SPOT (3) TM (4) ATLAS	(1) Town of Arkham, northeastern Toronto, Canada (2) Lucknow, Uttar Pradesh, India (3) Minneapolis, St. Paul, Minnesota (4) Baton Rouge, Louisiana	(1) Gong and Howarth, 1990 (2) Shaban and Dikshot, 2001 (3) Stuckens *et al.*, 2000 (4) Myint, 2001
4	Incorporation of ancillary data	(1) TM, zoning data, and housing densities (2) TM image and road density (3) SPOT HRV(XS), TM, census data	(1) Beaver Dam, Wisconsin (2) Beijing, China (3) Four medium-sized settlements in United Kingdom: Bristol, Swindon, Norwich, and Peterborough	(1) Harris and Ventura, 1995 (2) Zhang *et al.*, 2002 (3) Mesev, 1998
5	Use of multisensor data	(1) TM and RADARSAT C-band (2) TM and SPOT-P band (3) AVIRIS and radar	(1) Kathmandu Valley, Nepal (2) Wasatch Front, Utah (3) Park City, Utah	(1) Haack *et al.*, 2002 (2) Gluch, 2002 (3) Chen *et al.*, 2003
6	Use of normalized difference built-up index	TM	Nanjing, China	Zha *et al.*, 2003
7	Use of expert system	TM	(1) Phoenix metropolitan area, Arizona (2) Salt Lake City, Utah	(1) Stefanov *et al.*, 2001 (2) Hung and Ridd, 2002
8	Reclassification	SPOT-1 HRV	Southeast London, England	Barnsley and Barr, 1996

Airborne Visible/Infrared Imaging Spectrometer (AVIRIS) and radar data (Chen, *et al.*, 2003). Table 1 summarizes some research efforts to improve urban LULC classification accuracies.

One of the major advances in urban LULC analysis is Ridd's (1995) vegetation—impervious surface—soil (V-I-S) model (Figure 1). It assumes that land cover in urban environments is a linear combination of three components: vegetation, impervious surface, and soil. This model provides a guideline for decomposing urban landscapes and a link for these components to remote sensing spectral characteristics. Several studies have adopted this model as a basis for understanding the urban environment. Ward, *et al.* (2000) used a hierarchical unsupervised classification scheme to classify four classes (water, forest, cleared, and urban) on a per-pixel basis and applied the approach to a TM image in southeast Queensland, Australia, based on the V-I-S model. An adjusted overall accuracy of 83 percent was achieved. Madhavan, *et al.* (2001) used an unsupervised classifier (ISODATA) to classify TM images into seven classes in the Bangkok Metropolitan area, Thailand. The V-I-S model proved to be useful for the classification, although the classification accuracy was not as high as expected due to the complexity of the study area. Rashed, *et al.* (2001) conducted spectral mixture analysis (SMA) of IRS-1C multispectral image to describe the anatomy of the Greater Cairo Region, Egypt, based on four image endmembers: vegetation, impervious surface, soil, and shade. A decision tree classifier (DTC) was then applied to the fraction images. The classification accuracy was found to be higher than the accuracy achieved using MLC and minimum distance classifiers. Phinn, *et al.* (2002) compared traditional image classification, interpretation of aerial photographs, and constrained linear SMA using a TM image in southeast Queensland, Australia, and found that the V-I-S fraction images derived from SMA provided better classification results than per-pixel classification and aggregated aerial photo interpretation. Wu and Murray (2003) used SMA to analyze impervious surface distribution in the metropolitan area of Columbus, Ohio, USA, and found that impervious surface can be estimated using a linear regression model of low and high albedo endmember fractions.

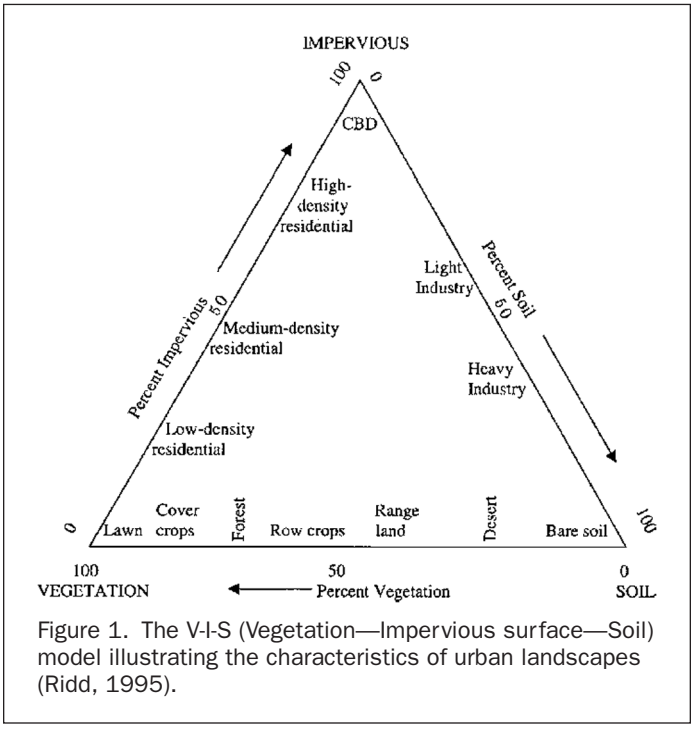

Figure 1. The V-I-S (Vegetation—Impervious surface—Soil) model illustrating the characteristics of urban landscapes (Ridd, 1995).

Although the V-I-S model has demonstrated usefulness for identifying and characterizing urban land cover patterns, its use in practice is constrained due to the following factors. First, the V-I-S model cannot explain all land cover types such as water and wetlands. Second, impervious surface in the V-I-S model cannot be easily identified as an endmember based on

remote sensing images (Wu and Murray, 2003) because impervious surface is a complex mixture of different materials, including concrete, asphalt, metals, plastic, and soils (Jensen, 2000). Finally, the V-I-S model excludes an important component in the mixed pixels, i.e., the shade. Shade, caused by tall buildings or trees, is an important factor affecting the spectral response patterns of urban landscapes and should be an essential consideration in analyzing urban landscapes. For medium-spatial resolution remotely sensed data, such as TM/ETM+, the central business district, light/heavy industry, high/medium density residential, and bare soils are difficult to differentiate using traditional digital image processing techniques. Recently SMA has attracted increasing interests in urban studies and has shown the potential for estimating impervious surface and vegetation abundance, and for improving urban land-cover classification (Rashed, *et al.*, 2001; Small, 2001; Phinn, *et al.*, 2002; Small, 2002; Wu and Murray, 2003). This paper evaluates the potential of SMA for characterizing an urban environment and for improving urban LULC classification accuracy.

Spectral Mixture Analysis

The linear SMA approach assumes that the spectrum measured by a sensor is a linear combination of the spectra of all components within the pixel (Adams, *et al.*, 1995; Roberts, *et al.*, 1998a). The mathematical model can be expressed as

$$R_i = \sum_{k=1}^{n} f_k R_{ik} + \varepsilon_i$$

where i is the number of spectral bands used; $k = 1, \ldots, n$ (number of endmembers); R_i is the spectral reflectance of band i of a pixel, which contains one or more endmembers; f_k is the proportion of endmember k within the pixel; R_{ik} is known as the spectral reflectance of endmember k within the pixel on band i, and ε_i is the error for band i. To solve f_k, the following conditions must be satisfied: (1) selected endmembers should be independent of each other, (2) the number of endmembers should be less than or equal to the spectral bands used, and (3) selected spectral bands should not be highly correlated.

It is well recognized that remotely sensed data, such as visible bands in Landsat TM/ETM+ data, are highly correlated between the adjacent spectral wavebands (Barnsley, 1999). Several techniques have been used to transform the data from highly correlated bands to an orthogonal subset. Principal component analysis (PCA) and minimum noise fraction (MNF) are the two most common transformations (Green, *et al.*, 1988; Boardman and Kruse, 1994; Jensen, 1996). The MNF transform contains two steps (ENVI, 2000): (1) de-correlation and rescaling of the noise in the data based on an estimated noise covariance matrix, producing transformed data in which the noise has unit variance and no band-to-band correlations; and (2) implementation of a standard PCA of the noise-whitened data. The result of MNF is a two-part dataset, one part associated with large eigenvalues and coherent eigenimages, and a complementary part with near-unity eigenvalues and noise-dominated images (ENVI, 2000). In the MNF transform, the noise is separated from the data by using only the coherent portions, thus improving spectral processing results. Previous studies have shown that use of MNF transform can improve the quality of fraction images (van der Meer and de Jong, 2000; Small, 2001; Lu, *et al.*, 2002; Small, 2002; Wu and Murray, 2003), and thus the MNF transform was used in this study.

Development of high-quality fraction images depends greatly on the selection of suitable endmembers. A variety of methods have been developed to determine endmembers. For example, endmembers can be obtained from (1) a spectral library, or field reflectance measurements; (2) the image itself (Quarmby, *et al.*, 1992; Settle and Drake, 1993) or high-order PCA eigenvectors (Boardman, 1993); (3) spectrally pure pixels identified using the Pixel Purity Index (PPI) (Boardman, *et al.*, 1995), which are selected manually by visualizing the PPI results in an N-dimensional visualizer with ENVI (ENVI, 2000); (4) manual endmember selection (Bateson and Curtiss, 1996), which is a multidimensional visualization technique for interactively exploring the mixing space in search of spectra to designate as endmembers; and (5) the combination of image and reference endmember selection methods. The combination approach involves a spectral alignment between image endmembers and reference endmembers, and a calibration to relate image endmembers to reference endmembers (Smith, *et al.*, 1990; Roberts, *et al.*, 1993). For most SMA applications, image endmembers are utilized because they can be easily obtained and can represent spectra measured at the same scale as the image data (Roberts, *et al.*, 1998a). The endmembers are regarded as the extremes in the triangles of an image scattergram. Hence, the image endmembers can be identified from the scatterplots of two spectral bands.

Study Area

The City of Indianapolis, located in Marion County, Indiana, with a population of over 800,000, was chosen as the study area (Figure 2). It is a key center of manufacturing, warehousing, distribution, and transportation. Situated in the middle of the country, Indianapolis possesses several other advantages that make it an appropriate choice. It has a single central city, and other large urban areas in the vicinity have not influenced its growth. The city is located on a flat plain and is relatively

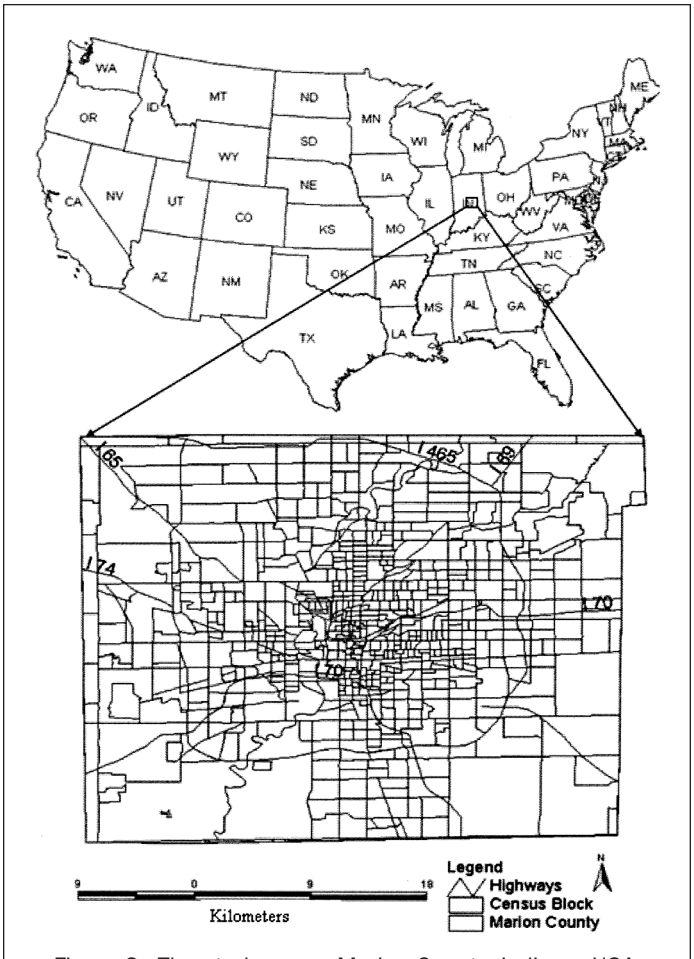

Figure 2. The study area—Marion County, Indiana, USA.

symmetrical, having possibilities of expansion in all directions. Like most American cities, Indianapolis is increasing in population and in area. The areal expansion is through encroachment into the adjacent agricultural and non-urban land. Certain decision-making forces, such as density of population, distance to work, property value, and income structure, encourage some sectors of metropolitan Indianapolis to expand faster than others. Analyzing the urban landscape structure and monitoring urban expansion and its environmental impacts in metropolitan Indianapolis is significant to understand, control, and plan its future development.

Method

The Landsat ETM+ image (L1G product of path 21, row 32) used in this study was acquired on 22 June 2000, under clear sky conditions. The data were radiometrically converted to at-sensor reflectance using image-based correction method (Markham and Barker, 1987). Although the L1G ETM+ data were geometrically corrected, its geometrical accuracy was not high enough for combining them with other high-resolution data sets. Hence, the image was further rectified to a common Universal Transverse Mercator coordinate system based on 1:24000 scale topographic maps and was resampled to a pixel size of 30 m by 30 m using the nearest-neighbor algorithm. A root mean square error of less than 0.5 pixels was obtained in the rectification. Following georectification, the MNF was applied to transform the ETM+ at-sensor reflectance data into a new coordinate set. The first four MNF components were used for spectral mixture analysis, and the last two were discarded due to their high proportion of noise contents.

Four types of endmembers were selected: shade, green vegetation (GV), impervious surfaces (such as building roofs and roads), and soils (including dry soil and dark soil). Endmembers were initially identified from the ETM+ image based on high-spatial resolution aerial photographs. The shade endmember was identified from the areas of clear and deep water, while GV was selected from the areas of dense grass and cover crops. Different types of impervious surfaces were selected from building roofs, airport runways, and highway intersections. Soils were selected from bare grounds in agricultural lands. Next, these initial endmembers were compared with those endmembers selected from the scatterplots of MNF1 and MNF2, and of MNF1 and MNF3. The endmembers with similar MNF spectra located at the extreme vertices of the scatterplots were selected. These endmembers were shade, GV, impervious surface, dry soil, and dark soil. An unconstrained least-squares regression solution was used to unmix the MNF components into fraction images.

To find the best quality of fraction images, different combinations of endmembers were tested. The combinations were: (1) four endmembers with shade, GV, impervious surface, and dark soil; (2) three endmembers with shade, GV, and impervious surface; (3) three endmembers with shade, GV, and dry soil; and (4) three endmembers with shade, GV, and dark soil. Visualization of fraction images, analysis of fraction characteristics of representative land cover types, and assessment of error images were conducted to determine which combination provided the best fractions for the study area.

High-spatial resolution aerial photographs were used to identify LULC sample plots. A total of 156 sample plots were identified, covering ten land-cover types: commercial and industrial urban area (hereafter, urban), high-intensity residential, low-intensity residential, bare soil, crop, grass, pasture, forest, wetland, and water. On average, 10 to 16 sample plots for each class were selected. A window size of three by three was applied to extract the fraction value for each plot. The average value and standard deviation were then calculated for each land cover class. A graph showing the fraction characteristics of selected LULC types was created to examine their different features in proportional compositions.

The MLC was applied to classify the fraction images into ten classes producing a classified image and a distance image. The distance image represents the result of the Mahalanobis distance between the measurement vector of the pixel and the mean vector of the pixel's class. Higher values in the distance image indicate greater spectral distances from the signature means for the classes to which they are assigned, i.e., more likely to be misclassified. A distance threshold was selected for each class to screen out the pixels that probably do not belong to that class, and was determined by examining interactively the histogram of each class in the distance image. Pixels with a distance value greater than the threshold were assigned a class value of zero in the thematic image.

The MLC is a parametric classifier that assumes normal or near normal spectral distribution for each feature of interest associated with an equal prior probability among the classes. Hence, training samples insufficient in number or non-representative of features of interest or having multimode distributions often lead to poor classification results because of inaccurate estimation of the mean vector and covariance matrix used in the MLC algorithm. In this situation, a non-parametric classifier, such as the DTC, is more suitable to use because no assumption is required. Therefore, the DTC approach was applied to reclassify the pixels that were set to zero based on the distance image. One critical step in using the DTC was to develop the threshold for each LULC type (Lu, *et al.*, 2003). These thresholds were identified based on the mean and standard deviation from the sample plots for each class. As a comparison, conventional supervised classification with MLC was also performed to classify the ETM+ image into the same categories of LULC classes using the same training sample data.

In urban landscape analysis, land use data are often more useful than land cover data because of their pertinence to planning and environmental management issues. Further derivation of land use data from a classified land cover image is often desirable. Having considered LULC characteristics and applications of the study area, the classified LULC image was finally merged into six classes: urban, residential, pasture and agricultural lands, grass, forest, and water. Pasture and cropland were combined since they have similar spectral responses and fractions. The wetland areas were very limited in extent, and were therefore merged into either forest or water depending on their characteristics. To improve the classification results between grass, pasture, and crops, the following rules were applied to the classified images developed using the SMA-based and MLC approaches, respectively: (1) when grasses were confused with pasture or crops in urban or residential areas, these pasture or crops were re-grouped as grass, and (2) when pasture or crops were misclassified as grass in the agricultural areas, they were merged into pasture-agricultural lands.

Accuracy assessment is considered an important part in LULC classification (Foody, 2002). The meaning and calculation for overall accuracy, producer's accuracy, user's accuracy, and kappa coefficient have been described extensively in the literature (Congalton and Mead, 1983; Hudson and Ramm, 1987; Congalton, 1991; Janssen and van der Wel, 1994; Kalkhan, *et al.*, 1997; Smits, *et al.*, 1999; Foody, 2002). The error matrix is the most frequently used method for quantitatively analyzing LULC classification accuracy and was used in this paper. The accuracies of the classified images were checked with a stratified random sampling method using a total of 150 samples. The reference data were collected from large-scale aerial photographs. Overall accuracy, producer's accuracy, and user's accuracy were calculated based on the error matrices for both classification results, as well as the KHAT statistic, kappa variance, and Z statistic.

Results

Fraction images derived from different combinations of endmembers were evaluated with visual interpretation and the error extent and distribution in the error fraction image. Because this study is more interested in characterizing urban LULC patterns than non-urban regions, the criteria to identify the best suitable fraction images are based on (1) high-quality fraction images in urban regions, (2) relatively low errors in the urban regions, and (3) the distinction among typical LULC types. Results indicated that a three-endmember combination of shade/GV/impervious surface provided a satisfactory result in urban areas, but a relatively poor performance for agricultural lands, especially for bare soils and pasture. In contrast, the combination of shade/GV/dark soil did not provide a satisfactory result for urban and residential areas but was suitable for agricultural areas. Four endmembers with shade/GV/impervious surface/dark soil or dry soil did not provide a satisfactory fraction result either, especially for urban and residential areas. The best combination of fractions was three endmembers with shade/GV/dry soil, which showed the best results for both urban areas and agricultural lands. Therefore, the fraction images derived from these three endmembers were used for LULC classification and were further examined in the following text.

The fractions represent the areal proportions of the endmembers within a pixel. Each land cover type has a distinct fraction composition. Figure 3 illustrates the three fraction images: shade, GV, and soil. As a comparison of fraction images and ETM+ image, the ETM+ panchromatic image was also included. In the shade fraction image, water appears very bright due to its high shade fraction. This is because shade endmember was selected from clear and deep water assuming that shade had similar spectral characteristics with water. Urban, residential, and forest have medium shade fraction values as indicated by their grey tone. Grass, pasture, and agricultural lands have a dark tone, indicative of the lowest fraction of shade. In the GV fraction image, forest and dense grass/pasture appear very bright, while residential areas and agricultural lands appear grey. Urban areas, bare soils, and water have a dark tone. The progression from areas of low to high GV fraction is apparent in the transition from high-density urban areas with minimal vegetation cover to low-density urban areas with a large proportion of vegetation cover. In the soil fraction image, the transition from urban to high residential to low residential is consistent with the tone change from white to bright grey to dark grey. Forest, water, and areas of dense grass/pasture exhibit a dark tone in the soil fraction image.

The fraction composition of each LULC type can be studied based on Figures 4a and 4b. The errors were not included in these figures due to their low values clustering near zero. These diagrams were constructed after examining fractions of 10 to 16 plots (3×3 window size) for each LULC type. Water possesses the highest shade fraction, but low GV and soil fractions. Forest and wetlands both have medium-high shade fractions and a high GV, but a low soil fraction. Residential areas show a medium shade fraction and relatively low GV and soil fractions. Grass and pasture share a similar fraction composition. Both are low in shade and soil fractions, but are high in the GV fraction. Croplands possess a relatively small shade fraction as well as soil fraction, in contrast with a medium GV fraction. Urban areas show the highest soil fraction among the LULC types. Bare soils in agricultural lands display a fraction composition similar to urban areas, except that bare soils have

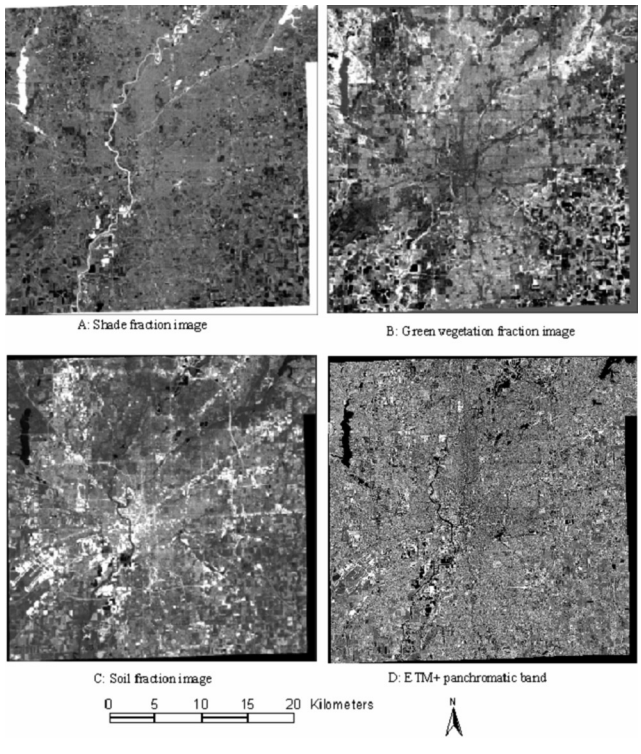

Figure 3. Characteristics of three fraction images (shade, green vegetation, and soil). The fractions were developed using a spectral mixture model based on the minimum noise transformed images and a comparison with the ETM+ panchromatic image.

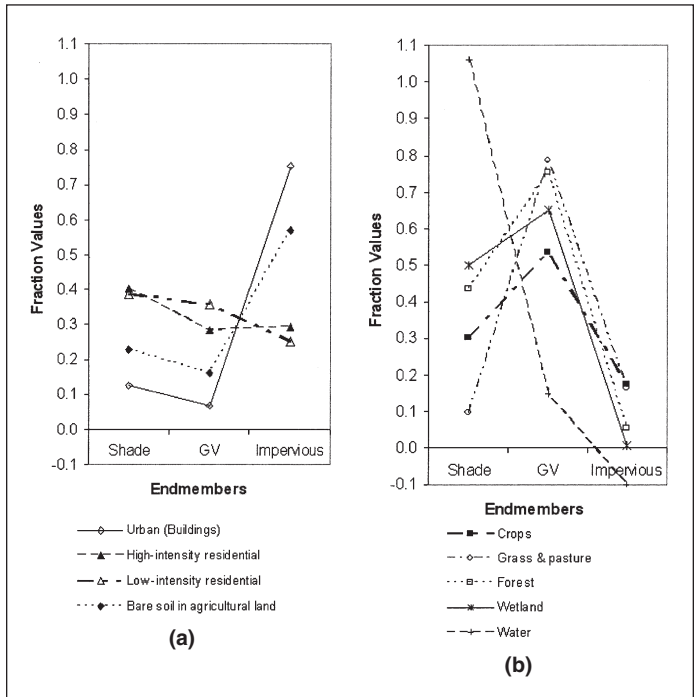

Figure 4. Comparison of fraction features among different land-use and land-cover types. 4a—Fraction compositions of urban buildings, high- and low-residential areas, and bare soil; 4b—Fraction compositions of cropland, grassland and pasture, forest, wetland, and water.

a bit higher shade and GV fractions. The soil fraction was the highest in urban and bare soils showing intermediate values in high- and low-intensity residential areas, low values for crop and pasture/grass, and lowest values in forest, wetland, and water. The shade fraction was highest for water, followed by wetland, forest, high- and low-residential areas. Crops, bare soils, and urban (buildings) all had a low shade fraction but higher than grass/pasture. Because the GV fraction is associated with vegetation abundance and biomass, it registered the highest value in grass/pasture/forest. Wetland/crops/low residential areas showed a medium GV fraction, whereas high-intensity residential/soil/water/urban (buildings) placed at the lowest level.

Based on the analysis of fraction characteristics of different LULC types, a conceptual model based on the V-I-S ternary diagram of Ridd (1995) was constructed to explain the relationship among the LULC types with respect to the fraction composition (Figure 5). Each land cover can be regarded as a linear combination of three components: shade, GV, and soil or impervious surface. For example, soil or impervious surface accounts for the majority of the bare soil or urban class. The GV fraction accounts for the majority of the dense grass and pasture. The shade fraction accounts for the majority of water and wetlands. Therefore, urban/bare soils, grass/pastures, and water/wetlands occupy the three vertices of the triangle. Crops, forest, and residential areas are transitional in the space of the fraction composition triangle, implying that they are composed of different proportions of GV, soil or impervious surface, and shade fractions. The proportion of crops depends largely on crop types and density, accounted for by GV and soil. Forest consists mainly of GV and shade fractions. Vegetation stand structure, species composition, and tree density affect their fractions. In residential areas, the fractions reflect the mixing result of their structure components, including buildings, trees, grass, and pavement. Therefore, in high residential areas, impervious surface and shade accounts for most of its composition, while in low residential areas, GV and shade fractions explain the majority of variation in the fraction composition. This conceptual model would be valuable as a guideline for urban LULC analysis using remotely sensed data.

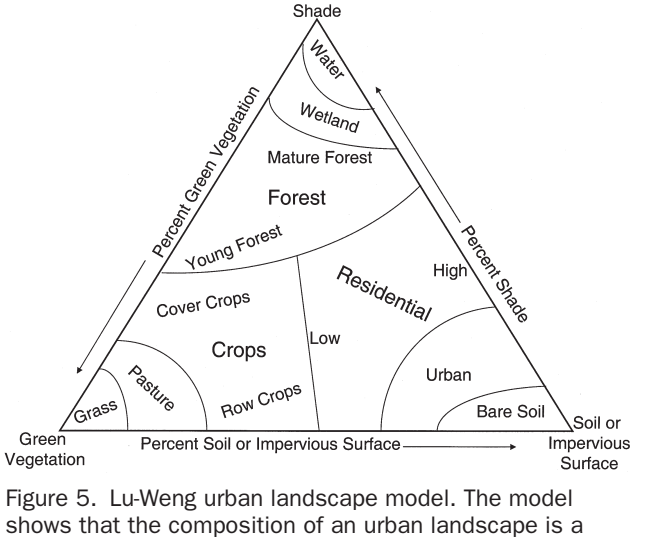

Figure 5. Lu-Weng urban landscape model. The model shows that the composition of an urban landscape is a linear combination of three fractions, shade, green vegetation, and soil/impervious surface. Various urban land cover types may be deciphered in terms of proportions of shade, green vegetation, and soil/impervious surface.

Plate 1 shows the resultant classification image from using the procedures described above. The main urban area is located in the center of the Marion County, while some small towns and one airport are distributed around the main urban area. Residential areas are distributed between the main urban areas and small towns. Forest is mainly seen in the surrounding areas, especially around the Eagle Creek Reservoir, and in Fort Harrison State Park along Fall Creek. Agricultural lands are located in the southeastern and southwestern parts of the study area. The overall accuracy of the LULC map was determined to be 89 percent using the SMA-based approach (Table 2). The classification performance of the SMA-based approach was a significant improvement (at a 98 percent confidence level) over MLC (overall accuracy: 80 percent). The kappa coefficients for the two maps were 0.86 and 0.73 respectively. Clearly, the LULC data derived from the SMA procedure have reasonably high accuracy and are sufficient for urban landscape analysis and growth detection. The main misclassifications arise from: (1) roads within urban and residential areas where some roads were classified as urban areas and others as residential depending on the road width and associated environmental conditions along the roads, (2) confusion between urban and dry bare soils in pasture and agricultural areas, and (3) confusion among grass, pasture, and some crops.

Discussion and Conclusions

Urban landscapes are complex and often difficult to classify. This study demonstrates that SMA is an effective approach for characterizing urban landscape patterns and for classifying urban LULC. Since many LULC types tend to occur as heterogeneous mixtures in the urban context, even when viewed at very fine spatial scales, utilization of SMA for improving LULC classification accuracy is especially valuable. This is particularly true when considering the fact that substantial increase in spatial resolution would produce compensating disadvantages, including increased cost and spectral variation of LULC types, which decreases the spectral separability of classes and reduces classification accuracy (Cao and Lam, 1997).

In SMA, endmember selection is a crucial step. The selection of suitable endmembers often involves an iterative process, i.e., selecting initial endmembers, refining these endmembers, evaluating fraction images, and then further refining endmembers. Finally, selected endmembers should be independent of each other. For a study area with complex landscape structures, such as those urban areas composed of residential, commercial and industrial uses, agricultural lands, and forest, identification and selection of proper endmembers for the whole study area is often not straightforward. Two possible approaches may be taken for effective derivation of endmembers in an intricate urban area: (1) stratification or (2) use of multiple endmembers.

Stratification of the whole study area into smaller regions of similar landscape structures may be necessary to facilitate the derivation of high-quality fraction images. For example, in a study area dominated by residential, commercial, and industrial uses, possible endmembers may be GV, shade, and impervious surface, while in an agriculture-dominated region, endmembers may be GV, shade, and soil. If an urban area under investigation has a large proportion of forests, then GV, shade, and non-photosynthetic vegetation (NPV) could be the most appropriate choices of endmembers for the forested areas. However, if GV, shade, impervious surface, soil, and NPV are used for the entire study area without stratification, the process for developing high-quality fraction images could be lengthy and technically difficult due to potentially high correlations among some endmembers, e.g., among impervious surfaces, soil, and NPV.

TABLE 2. COMPARISON OF CLASSIFICATION ACCURACY ASSESSMENT RESULTS BETWEEN THE SMA-BASED CLASSIFIER AND MLC

Method	Classified Data	Reference Data						Ref. Totals	Class. Totals	Number Correct	PA	UA	Kappa
		Urban	Res.[a]	Forest	Grass	PS-AG[b]	Water						
SMA	Urban	21	0	0	0	1	0	26	22	21	80.77%	95.45%	0.945
	Residential	3	56	0	1	2	0	57	62	56	98.25%	90.32%	0.844
	Forest	0	0	9	0	0	0	11	9	9	81.82%	100.00%	1.000
	Grass	0	1	1	28	1	0	32	31	28	87.50%	90.32%	0.877
	PS-AG	2	0	1	3	16	0	20	22	16	80.00%	72.73%	0.685
	Water	0	0	0	0	0	4	4	4	4	100.00%	100.00%	1.000
	Overall Classification Accuracy = 89.33% (i.e., 134/150), Overall Kappa Statistics = 0.8575												
MLC	Urban	19	1	0	0	1	0	26	21	19	73.08%	90.48%	0.885
	Residential	7	56	0	7	2	0	57	72	56	98.25%	77.78%	0.642
	Forest	0	0	8	0	0	0	11	8	8	72.73%	100.00%	1.000
	Grass	0	0	3	18	2	0	32	23	18	56.25%	78.26%	0.724
	PS-AG	0	0	0	7	15	0	20	22	15	75.00%	68.18%	0.633
	Water	0	0	0	0	0	4	4	4	4	100.00%	100.00%	1.000
	Overall Classification Accuracy = 80.00% (i.e., 120/150), Overall Kappa Statistics = 0.7284												
Note	Variance for SMA = 0.001115; Variance for MLC = 0.001923; Z statistics = 2.342654; Significant at 98% confidence level												

Note: Res.[a]—Residential; PS-AG[b]—pasture and agricultural lands.
Ref.—Reference; Class.—Classified
PA and UA—producer's accuracy and user's accuracy, respectively.

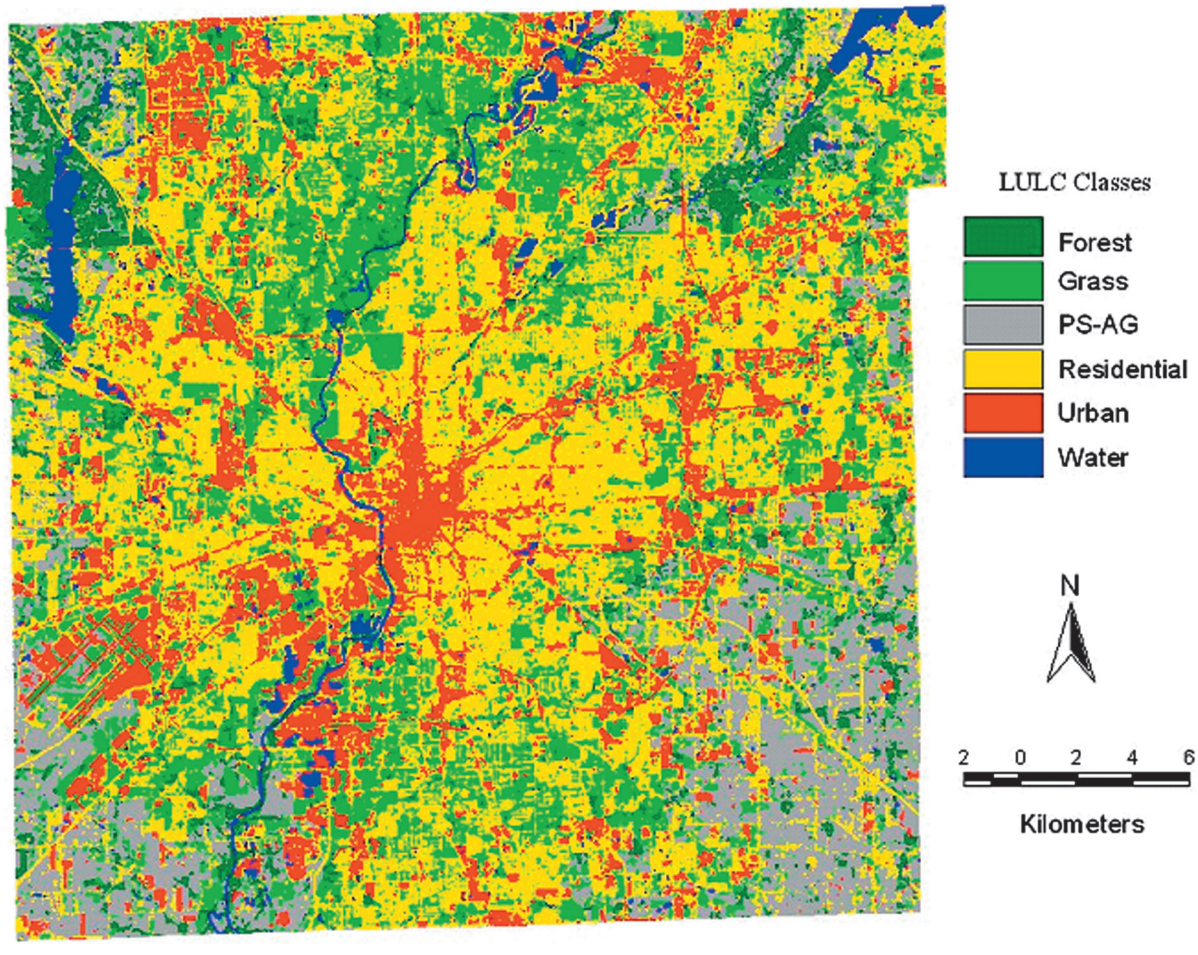

Plate 1. Urban land-use and land-cover classification image of Marion County, Indiana, USA based on a SMA-based approach.

For most SMA studies, limited endmembers, i.e., three or four endmembers, were used (Roberts, *et al.*, 1998a; Small, 2001; Wu and Murray, 2003). However, in a complex landscape, a limited number of endmembers may not account for the spectral variability of the landscape and cannot tackle the mixed pixel problem. In urban regions, because of the complexity of impervious surfaces, identifying suitable impervious surfaces as endmembers useful in SMA is often difficult, and the impervious surfaces tend to be confused with soils, although some previous research used impervious surface as an endmember (Rashed, *et al.*, 2001; Phinn, *et al.*, 2002). Moreover, different urban areas may have different impervious surface types. Hence, a possible method is to use multiple endmember models (Roberts, *et al.*, 1998b). The multiple endmember SMA approach permits a large number of endmembers to be modeled across a scene and has shown a better performance than the standard SMA approach (Painter, *et al.*, 1998; Roberts, *et al.*, 1998b; Okin, *et al.* 2001). This approach starts with a series of candidate two-endmember models and then evaluates each model based on three criteria of fraction values, root mean square error, and residual threshold, and finally produces fraction images with the lowest error (Roberts, *et al.*, 1998b). The multiple-endmember SMA approach may be more suitable for use in urban landscapes.

A comparison of the V-I-S model by Ridd (1995) and the new conceptual model developed in this paper (Lu-Weng Model) will give some insights into urban LULC patterns. In the V-I-S model, vegetation, impervious surface, and soil are regarded as three fundamental components, but in practice, impervious surface is a complex combination of different materials, and is difficult to identify because it may vary greatly in different locations. On the other hand, shade is an important component captured by optical remote sensors. Therefore, the shade component is included in the Lu-Weng model. Impervious surface, shade, and vegetation are considered essential components in the urban area; while in a non-urban region, soil, vegetation, and shade can account for the spectral variability. Given the importance of impervious surfaces in urban landscapes and their confusion with soils, further research efforts are necessary to examine the fractional characteristics of soils and impervious surfaces.

Another important contribution SMA makes to image processing techniques is that it provides a suitable model to decompose the spectral mixtures of L-resolution data such as TM/ETM+. Thus, a more realistic representation of the true nature of a surface is possible compared with that provided by the assignment of a single dominant class to every pixel by statistical models (Campbell, 2002). This research indicates that SMA approach is suitable to solve the mixture problem in the L-resolution data and provided better classification results in the urban environments than traditional per-pixel based maximum likelihood classifier. Fraction images may have a great potential for improving classification quality when combined with temperature and other GIS ancillary data, population, and other social-economic variables. This study reveals that although fraction images can be successfully used for urban LULC classification, some confusions still exist. Further studies should be encouraged by incorporation of fraction images and some ancillary data such as census, or by a combination of fraction images with texture information, or by fusion of multisensor data such as TM/ETM+ and radar imagery, so classification accuracy should be improved.

Acknowledgments

The authors wish to thank the three anonymous reviewers for their constructive comments and suggestions. We further acknowledge the financial supports of University Research Committee at Indiana State University through the grant #UNR184 and from the Center for the Study of Institutions, Population, and Environmental Change (CIPEC), Indiana University, through the National Science Foundation (Grant 99-06826).

References

Adams, J.B., D.E. Sabol, V. Kapos, R.A. Filho, D.A. Roberts, M.O. Smith, and A.R. Gillespie, 1995. Classification of multispectral images based on fractions of endmembers: Application to land cover change in the Brazilian Amazon, *Remote Sensing of Environment*, 52:137–154.

Barnsley, M.J., and S.L. Barr, 1996. Inferring urban land use from satellite sensor images using kernel-based spatial reclassification, *Photogrammetric Engineering & Remote Sensing*, 62:949–958.

Barnsley, M.J., 1999. Digital remote sensing data and their characteristics, *Geographical Information Systems: Principles, Techniques, Applications, and Management* (Second Edition) (P. Longley, M. Goodchild, D.J. Maguire and D.W. Rhind, editors), John Wiley & Sons, New York, N.Y., pp. 451–466.

Bateson, A., and B. Curtiss, 1996. A method for manual endmember selection and spectral unmixing, *Remote Sensing of Environment*, 55:229–243.

Boardman, J.W., 1993. Automated spectral unmixing of AVIRIS data using convex geometry concepts, *Summaries of the Fourth JPL Airborne Geoscience Workshop*, JPL Publication 93-26, NASA Jet Propulsion Laboratory, Pasadena, Calif., pp. 11–14.

Boardman, J.W., and F.A. Kruse, 1994. Automated spectral analysis: A geological example using AVIRIS data, north Grapevine Mountains, Nevada, *Proceedings*, *ERIM Tenth Thematic Conference on Geologic Remote Sensing*, Ann Arbor, MI, pp. 407–418.

Boardman, J.M., F.A. Kruse, and R.O. Green, 1995. Mapping target signature via partial unmixing of AVIRIS data, *Summaries of the Fifth JPL Airborne Earth Science Workshop*, JPL Publication 95–1, NASA Jet Propulsion Laboratory, Pasadena, Calif., pp. 23–26.

Campbell, J.B., 2002. *Introduction to Remote Sensing* (3rd Edition), The Guilford Press, New York, N.Y., 621 p.

Cao, C., and N.S.N. Lam, 1997. Understanding the scale and resolution effects in remote sensing and GIS, *Scale in Remote Sensing and GIS*, (D.A. Quattrochi and M.F. Goodchild, editors), Lewis Publishers, Boca Raton, FL, pp. 57–72.

Chen, C.-M., G.F. Hepner, and R.R. Forster, 2003. Fusion of hyperspectral and radar data using the IHS transformation to enhance urban surface features, *ISPRS Journal of Photogrammetry and Remote Sensing*, 58:19–30.

Chen, S., S. Zheng, and C. Xie, 2000. Remote sensing and GIS for urban growth in China, *Photogrammetric Engineering & Remote Sensing*, 66:593–598.

Congalton, R.G., 1991. A review of assessing the accuracy of classification of remotely sensed data, *Remote Sensing of Environment*, 37:35–46.

Congalton, R.G., and R.A. Mead, 1983. A quantitative method to test for consistency and correctness in photo interpretation, *Photogrammetric Engineering & Remote Sensing*, 49:69–74.

Cracknell, A.P., 1998. Synergy in remote sensing—what's in a pixel? *International Journal of Remote Sensing*, 19:2025–2047.

ENVI, 2000. *ENVI User's Guide*. Research Systems Inc., Boulder, Colorado, 930 p.

Epstein, J., K. Payne, and E. Kramer, 2002. Techniques for mapping suburban sprawl, *Photogrammetric Engineering & Remote Sensing*, 63:913–918.

Fisher, P., 1997. The pixel: A snare and a delusion, *International Journal of Remote Sensing*, 18:679–685.

Foody, G.M., 2002. Status of land cover classification accuracy assessment, *Remote Sensing of Environment*, 80:185–201.

Gong, P., and P.J. Howarth, 1990. The use of structure information for improving land-cover classification accuracies at the rural-urban fringe, *Photogrammetric Engineering & Remote Sensing*, 56:67–73.

Gluch, R., 2002. Urban growth detection using texture analysis on merged Landsat TM and SPOT-P data, *Photogrammetric Engineering & Remote Sensing*, 68:1283–1288.

Green, A.A., M. Berman, P. Switzer, and M.D. Craig, 1988. A transformation for ordering multispectral data in terms of image quality with implications for noise removal, *IEEE Transactions on Geoscience and Remote Sensing*, 26:65–74.

Haack, B.N., E.K. Solomon, M.A. Bechdol, and N.D. Herold, 2002. Radar and optical data comparison/integration for urban delineation: A case study, *Photogrammetric Engineering & Remote Sensing*, 68:1289–1296.

Harris, P.M., and S.J. Ventura, 1995. The integration of geographic data with remotely sensed imagery to improve classification in an urban area, *Photogrammetric Engineering & Remote Sensing*, 61:993–998.

Hudson, W.D., and C.W. Ramm, 1987. Correct formulation of the Kappa coefficient of agreement, *Photogrammetric Engineering & Remote Sensing*, 53:421–422.

Hung, M., and M.K. Ridd, 2002. A subpixel classifier for urban land-cover mapping based on a maximum-likelihood approach and expert system rules, *Photogrammetric Engineering & Remote Sensing*, 68:1173–1180.

Janssen, L.F.J., and F.J.M. van der Wel, 1994. Accuracy assessment of satellite derived land-cover data: A review, *Photogrammetric Engineering & Remote Sensing*, 60:419–426.

Jensen, J.R., 1996. *Introductory Digital Image Processing: A Remote Sensing Perspective* (2nd Edition), Prentice Hall, Upper Saddle River, New Jersey, 318 p.

Jensen, J.R., 2000. *Remote Sensing of the Environment: An Earth Resource Perspective,* Prentice Hall, Upper Saddle River, New Jersey, 544 p.

Kalkhan, M.A., R.M. Reich, and R.L. Czaplewski, 1997. Variance estimates and confidence intervals for the Kappa measure of classification accuracy, *Canadian Journal of Remote Sensing*, 23:210–216.

Lo, C.P., 1995. Automated population and dwelling unit estimation from high-resolution satellite images: A GIS approach, *International Journal of Remote Sensing*, 16:17–34.

Lo, C.P., D. Quattrochi, and J. Luvall, 1997. Application of high-resolution thermal infrared remote sensing and GIS to assess the urban heat island effect, *International Journal of Remote Sensing*, 18:287–304.

Lu, D., M. Batistella, and E. Moran, 2002. Linear Spectral Mixture Analysis of TM Data for Land-use and Land-Cover Classification in Rondonia, Brazilian Amazon, *Proceedings of the ISPRS Commission IV Symposium: Geospatial Theory, Processing and Applications*, (C. Armenakis and Y.C. Lee, editors), Published by Center for Topographic Information Mapping Services Branch, Geomatics Canada, Department of Natural Resources Canada, Ottawa, Canada, pp. 557–562.

Lu, D., E. Moran, and M. Batistella, 2003. Linear mixture model applied to Amazonian vegetation classification, *Remote Sensing of Environment*, 87:456–469.

Madhavan, B.B., S. Kubo, N. Kurisaki, and T.V.L.N. Sivakumar, 2001. Appraising the anatomy and spatial growth of the Bangkok Metropolitan area using a vegetation-impervious-soil model through remote sensing, *International Journal of Remote Sensing*, 22:789–806.

Markham, B.L., and J.L. Barker, 1987. Thematic Mapper bandpass solar exoatmospheric irradiances, *International Journal of Remote Sensing*, 8:517–523.

Mesev, V., 1998. The use of census data in urban image classification, *Photogrammetric Engineering & Remote Sensing*, 64:431–438.

Myint, S.W., 2001. A robust texture analysis and classification approach for urban land-use and land-cover feature discrimination, *Geocarto International*, 16:27–38.

Okin, G.S., D.A. Roberts, B. Murray, and W.J. Okin, 2001. Practical limits on hyperspectral vegetation discrimination in arid and semiarid environments, *Remote Sensing of Environment,* 77: 212–225.

Painter, T.H., D.A. Roberts, R.O. Green, and J. Dozier, 1998. The effects of grain size on spectral mixture analysis of snow-covered area from AVIRIS data, *Remote Sensing of Environment,* 65: 320–332.

Phinn, S., M. Stanford, P. Scarth, A.T. Murray, and P.T. Shyy, 2002. Monitoring the composition of urban environments based on the vegetation-impervious surface-soil (VIS) model by subpixel analysis techniques, *International Journal of Remote Sensing*, 23:4131–4153.

Quarmby, N.A., J.R.G. Townshend, J.J. Settle, and K.H. White, 1992. Linear mixture modeling applied to AVHRR data for crop area estimation, *International Journal of Remote Sensing*, 13:415–425.

Quattrochi, D.A., J.C. Luvall, D.L. Rickman, M.G. Estes, C.A. Laymon, and B.F. Howell, 2000. A decision support information system for urban landscape management using thermal infrared data, *Photogrammetric Engineering & Remote Sensing*, 66:1195–1207.

Rashed, T., J.R. Weeks, M.S. Gadalla, and A.G. Hill, 2001. Revealing the anatomy of cities through spectral mixture analysis of multisepctral satellite imagery: A case study of the Greater Cairo region, Egypt, *Geocarto International*, 16:5–15.

Ridd, M.K., 1995. Exploring a V-I-S (Vegetation-Impervious Surface-Soil) model for urban ecosystem analysis through remote sensing: Comparative anatomy for cities, *International Journal of Remote Sensing*, 16:2165–2185.

Roberts, D.A., M.O. Smith, and J.B. Adams, 1993. Green vegetation, non-photosynthetic vegetation, and soils in AVIRIS data, *Remote Sensing of Environment*, 44:255–269.

Roberts, D.A., G.T. Batista, J.L.G. Pereira, E.K. Waller, and B.W. Nelson, 1998a. Change identification using multitemporal spectral mixture analysis: Applications in eastern Amazônia, *Remote Sensing Change Detection: Environmental Monitoring Methods and Applications* (R.S. Lunetta and C.D. Elvidge, editors), Ann Arbor Press, Ann Arbor, Mich., pp. 137–161.

Roberts, D.A., M. Gardner, R. Church, S. Ustin, G. Scheer, and R.O. Green, 1998b, Mapping chaparral in the Santa Monica mountains using multiple endmember spectral mixture models, *Remote Sensing of Environment,* 65:267–279.

Settle, J.J., and N.A. Drake, 1993. Linear mixing and the estimation of ground cover proportions, *International Journal of Remote Sensing*, 14:1159–1177.

Shaban, M.A., and O. Dikshit, 2001. Improvement of classification in urban areas by the use of textural features: The case study of Lucknow city, Uttar Pradesh, *International Journal of Remote Sensing*, 22:565–593.

Small, C., 2001. Estimation of urban vegetation abundance by spectral mixture analysis, *International Journal of Remote Sensing*, 22:1305–1334.

Small, C., 2002. Multitemporal analysis of urban reflectance, *Remote Sensing of Environment*, 81:427–442.

Smith, M.O., S.L. Ustin, J.B. Adams, and A.R. Gillespie, 1990. Vegetation in Deserts: I. A regional measure of abundance from multispectral images, *Remote Sensing of Environment*, 31:1–26.

Smits, P.C., S.G. Dellepiane, and R.A. Schowengerdt, 1999. Quality assessment of image classification algorithms for land-cover mapping: A review and a proposal for a cost-based approach, *International Journal of Remote Sensing*, 20:1461–1486.

Stefanov, W.L., M.S. Ramsey, and P.R. Christensen, 2001. Monitoring urban land cover change: An expert system approach to land cover classification of semiarid to arid urban centers, *Remote Sensing of Environment,* 77:173–185.

Strahler, A.H., C.E. Woodcock, and J.A. Smith, 1986. On the nature of models in remote sensing, *Remote Sensing of Environment,* 70:121–139.

Stuckens, J., P.R. Coppin, and M.E. Bauer, 2000. Integrating contextual information with per-pixel classification for improved land cover classification, *Remote Sensing of Environment,* 71:282–296.

Thomson, C.N., and P. Hardin, 2000. Remote sensing/GIS integration to identify potential low-income housing sites, *Cities*, 17:97–109.

Van der Meer, F., and S.M. de Jong, 2000. Improving the results of spectral unmixing of Landsat Thematic Mapper imagery by enhancing the orthogonality of end-members, *International Journal of Remote Sensing,* 21:2781–97.

Ward, D., S.R. Phinn, and A.L. Murray, 2000. Monitoring growth in rapidly urbanizing areas using remotely sensed data, *Professional Geographer*, 53:371–386.

Weng, Q., 2001. A remote sensing-GIS evaluation of urban expansion and its impact on surface temperature in the Zhujiang Delta, China, *International Journal of Remote Sensing*, 22:1999–2014.

Wu, C., and A.T. Murray, 2003. Estimating impervious surface distribution by spectral mixture analysis, *Remote Sensing of Environment*, 84:493–505.

Zha, Y., J. Gao, and S. Ni, 2003. Use of normalized difference built-up index in automatically mapping urban areas from TM imagery, *International Journal of Remote Sensing*, 24:583–594.

Zhang, J., and G.M. Foody, 2001. Fully-fuzzy supervised classification of sub-urban land cover from remotely sensed imagery: Statistical neural network approaches, *International Journal of Remote Sensing*, 22:615–628.

Zhang, Q., J. Wang, X. Peng, P. Gong, and P. Shi, 2002. Urban built-up land change detection with road density and spectral information from multitemporal Landsat TM data, *International Journal of Remote Sensing*, 23:3057–3078.

Zhu, G., and D.G. Blumberg, 2002. Classification using ASTER data and SVM algorithms: The case study of Beer Sheva, Israel, *Remote Sensing of Environment*, 80:233–240.

(Received 07 February 2003; accepted 24 July 2003; revised 22 August 2003)